fractal and fractional

MDPI

Article

Joint Battery State of Charge Estimation Method Based on a Fractional-Order Model with an Improved Unscented Kalman Filter and Extended Kalman Filter for Full Parameter Updating

Jingjin Wu †, Yuhao Li †, Qian Sun, Yu Zhu, Jiejie Xing and Lina Zhang *

School of Mechanical and Electrical Engineering, Hainan University, Haikou 570228, China; jingjin.wu@hainanu.edu.cn (J.W.); yuhao998@foxmail.com (Y.L.); qian_sun100@163.com (Q.S.); zhuyu221224@163.com (Y.Z.); 994199@hainanu.edu.cn (J.X.)

* Correspondence: zhanglina_6789@163.com

† These authors contributed equally to this work.

Abstract: State estimation of batteries is crucial in battery management systems (BMSs), particularly for accurately predicting the state of charge (SOC), which ensures safe and efficient battery operation. This paper proposes a joint SOC estimation method based on a fractional-order model, utilizing a multi-innovation full-tracking adaptive unscented Kalman filter (FOMIST-AUKF-EKF) combined with an extended Kalman filter (EKF) for online parameter updates. The fractional-order model more effectively represents the battery's dynamic characteristics compared to traditional integer-order models, providing a more precise depiction of electrochemical processes and nonlinear behaviors. It offers superior modeling for long-memory effects, complex dynamics, and aging processes, enhancing adaptability to aging and nonlinear characteristics. Comparative results indicate a maximum end-voltage error reduction of 0.002 V with the fractional-order model compared to the integer-order model. The multi-innovation technology increases filter robustness against noise by incorporating multiple historical observations, while the full-tracking adaptive strategy dynamically adjusts the noise covariance matrix based on real-time data, thus enhancing estimation accuracy. Furthermore, EKF updates battery parameters (e.g., resistance and capacitance) in real time, correcting model errors and improving SOC prediction accuracy. Simulation and experimental validation show that the proposed method significantly outperforms traditional UKF-based SOC estimation techniques in accuracy, stability, and adaptability. Specifically, under varying conditions such as NEDC and DST, the method demonstrates excellent robustness and practicality, with maximum SOC estimation errors of 0.27% and 0.67%, respectively.

Keywords: fractional-order model; state of charge (SOC); battery management system; multi-innovation; online update of battery parameters

Citation: Wu, J.; Li, Y.; Sun, Q.; Zhu, Y.; Xing, J.; Zhang, L. Joint Battery State of Charge Estimation Method Based on a Fractional-Order Model with an Improved Unscented Kalman Filter and Extended Kalman Filter for Full Parameter Updating. *Fractal Fract.* **2024**, *8*, 695. https://doi.org/10.3390/fractalfract8120695

Academic Editor: Costas Psychalinos

Received: 1 October 2024
Revised: 14 November 2024
Accepted: 20 November 2024
Published: 26 November 2024

1. Introduction

With the growing global demand for renewable energy, batteries are being increasingly used as energy storage devices in electric vehicles, renewable energy generation systems, and energy storage systems [1,2]. The battery management system (BMS) plays a critical role in ensuring safety, reliability, and longevity of batteries [3]. A core function of the BMS is the accurate estimation of the state of charge (SOC), which indicates the remaining charge. However, accurately estimating SOC is challenging due to the complex electrochemical processes within batteries, varying operating conditions, and effects of aging. Fractional-order models offer a novel approach to address these challenges by providing a more precise representation of battery dynamics, improving SOC prediction accuracy, and optimizing overall BMS performance. Traditional SOC estimation methods, such as model-based approaches using voltage and current measurements [4,5], rely on sensor data but often

struggle with inaccuracies due to noise and battery system nonlinearity [6]. The fractional-order model (FOM) has gained prominence due to its ability to capture nonlinearities and long-term memory effects [7]. By utilizing fractional-order calculus, FOMs provide a more accurate and flexible representation of complex electrochemical behavior, particularly for aging, polarization, and diffusion [7–9].

In recent years, a variety of model-based predictive methods have emerged, with model predictive control (MPC) primarily being used for system control by optimizing control inputs to achieve dynamic control over systems [10,11]. This approach can be applied in battery management systems (BMSs) to balance battery charging currents and also in the design of charging and discharging strategies according to battery aging trends under various conditions. Although MPC offers significant advantages in control and optimization, it is mainly used for optimizing control inputs rather than direct SOC estimation, making it unsuitable for SOC estimation. Neural-network-based predictive models, however, can achieve highly accurate SOC predictions using historical data, particularly under complex battery conditions, where they can adapt quickly to changes over time [12]. Nevertheless, data-driven methods have high computational demands, and neural network models require substantial historical data for training to ensure sufficient generalization capabilities. In the estimation of battery SOC, the Kalman filter [13] and its extended versions, such as the extended Kalman filter (EKF) [14] and the unscented Kalman filter (UKF) [15], are widely utilized due to their ability to handle nonlinear systems. However, the EKF relies on first-order Taylor expansion for linearization, which introduces significant linearization errors when applied to highly nonlinear systems. In contrast, the UKF addresses this issue by employing the unscented transformation (UT) [16,17], resulting in improved performance in estimating the SOC of batteries [18]. To overcome the limitations of traditional equivalent circuit and electrochemical models, the impedance model based on fractional-order theory has been explored. Its parameters are determined using an evolutionary optimization method, leading to the development of the fractional-order unscented Kalman kilter (FOUKF) method, which is more suitable for tackling large-scale nonlinear problems. Jin et al. [19] demonstrated that the error in SOC estimation using the fractional-order model (FOM) was consistently lower than that of the DPM-based SOC estimation method. Lai et al. [20] developed an SOC estimator and formulated a synergistic estimation method for both SOC and state of power (SOP), verifying its effectiveness under dynamic operating conditions. However, the error in these methods tends to increase as the battery ages, primarily due to the lack of online updating for the parameters in the fractional-order model.

Addressing the time-varying characteristics of battery systems and mitigating measurement noise are crucial for enhancing estimation accuracy and robustness [21]. This paper introduces a method that combines a fractional-order multiple innovation strong tracking adaptive unscented Kalman filter with an extended Kalman filter for joint estimation (FOMIST-AUKF-EKF). To improve SOC estimation accuracy and stability, this approach integrates fractional-order models with multiple innovation filtering, adaptive unscented Kalman filtering, and strong tracking techniques. Unlike single innovation filtering, multiple innovation filtering utilizes observations across multiple time steps, thereby improving robustness against noise [22,23]. Moreover, the Strong Tracking Filter (STF) strengthens the filter's ability to react to sudden shifts in the system state [24].

Wang et al. introduced a compensated adaptive model leveraging a strong tracking filter, but the predictive accuracy of this approach diminishes as parameter dimensions increase [25]. Although it accurately captures abrupt changes in lithium-ion batteries, it lacks considerations for computational cost and parameter dimensionality. Incorporating an adaptive mechanism allows the noise covariance matrix to adjust dynamically based on real-time measurements, thereby enhancing estimation performance across varied operating conditions [26]. Fan et al. [27] developed an adaptive traceless Kalman filtering method that optimized the AUKF's estimation accuracy by determining the ideal covariance matching (CM) window size. To address uncertainties in lithium-ion battery noise, Fu et al. [28]

proposed an adaptive extended Kalman filter (AEKF), demonstrating that the AEKF is more resistant to interference compared to conventional EKF.

In this study, the EKF is applied for real-time parameter updates of the battery model shown in Figure 1. Through first-order linearization, the EKF facilitates dynamic parameter adjustments, even in complex battery systems. Integrating the EKF with fractional-order models allows for real-time corrections of battery parameters, providing an estimation framework that captures the battery's nonlinear characteristics and adapts to parameter variations across different operating conditions, thus ensuring sustained accuracy. Zhang et al. [29] explored the multiscale effect of fractional-order models in parameter identification, implementing the model by isolating distinct features for online parameter identification. Beelen et al. [30] proposed an approach for simultaneous SOC- and EKF-based parameter estimation, achieving an error margin of 0.5%. Compared to traditional SOC estimation methods, the FOMIST-AUKF-EKF approach offers several distinct advantages, including:

(1) A proposed method for estimating battery SOC based on a fractional-order model, which better explains electrochemical behavior and long-term memory effects.
(2) Improved estimation accuracy and robustness in the battery's dynamic response through multi-innovation filtering and full-tracking strong tracking. The introduction of an adaptive UKF further enhances the system's ability to adjust to model uncertainties and noise variations.
(3) Online updates of the battery's full parameters using the EKF, which dynamically corrects the critical parameters in the battery model, ensuring long-term accuracy in SOC estimation.

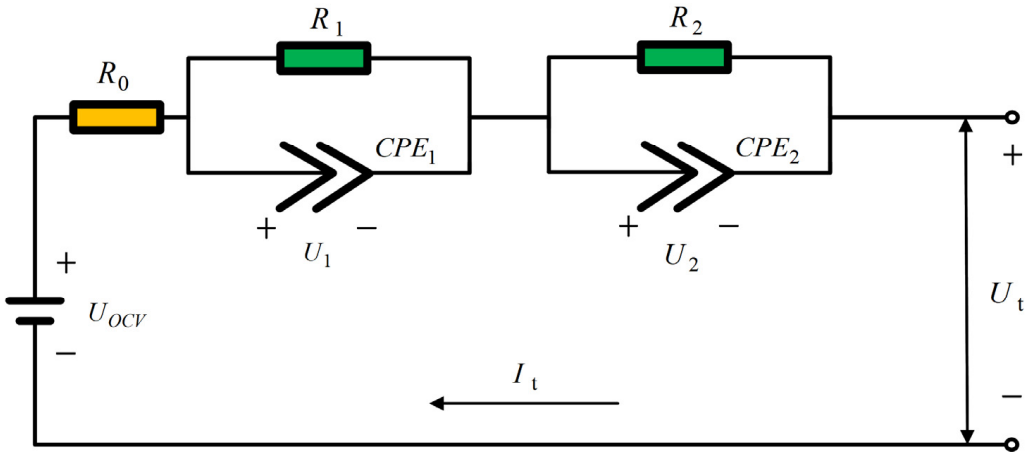

Figure 1. Fractional-order second-order RC model.

The remainder of this paper is organized as follows: Section 2 introduces the concept of fractional calculus in battery equivalent models. Based on fractional calculus, a fractional-order second-order RC model is established, along with the state space equations, and the results of parameter identification and accuracy are discussed. Section 3 presents the computational process of the FOMIST-AUKF-EKF algorithm. Section 4 analyzes and verifies the computational accuracy of the FOMIST-AUKF-EKF algorithm. Lastly, Section 5 summarizes the experimental conclusions.

2. Fractional-Order Modeling

2.1. Fractional-Order Calculus

With the increasing demand for accurate SOC estimation, the need for a precise equivalent model has become more essential. Fractional-order models provide an effective approach for capturing the dynamic characteristics of batteries, such as memory effects and time delays—complexities that traditional integer-order models struggle to accurately represent.

The three most popular definitions of fractional-order calculus are as follows: the Caputo definition [31], the Riemann–Liouville (RL) definition [32], and the Grünwald–Letnikov (GL) definition [33].

Caputo derivative definition:

$$D_t^\alpha f(t) = \frac{1}{\Gamma(1-\alpha)} \int_0^t \frac{f'(\tau)}{(t-\tau)^\alpha} d\tau \quad 0 < \alpha < 1 \tag{1}$$

where α is the fractional-order operator, Γ() is the gamma function, τ and t are the boundaries of the operation. Caputo derivatives are suitable for initial value problems, where initial conditions are easy to handle, and are commonly used in physics and engineering [34].

Riemann–Liouville (RL) definition:

$$D_t^\alpha f(t) = \frac{1}{\Gamma(n-\alpha)} \frac{d^n}{dt^n} \int_0^t \frac{f(\tau)}{(t-\tau)^{\alpha-n+1}} d\tau \quad n-1 < \alpha < n \tag{2}$$

where n is a positive integer without an initial t condition. Riemann–Liouville has a wide range of applications in theoretical studies and was one of the first definitions of fractional-order calculus to be proposed.

Grünwald–Letnikov (GL) definition:

$$D_t^\alpha f(t) = \lim_{h \to 0} \frac{1}{h^\alpha} \sum_{j=0}^{\infty} (-1)^j \binom{\alpha}{j} f(t-jh) \tag{3}$$

where h represents the sampling interval and $\binom{\alpha}{j}$ is the Newtonian binomial coefficient, as shown in Equation (4).

$$\binom{\alpha}{j} = \begin{cases} \frac{\alpha!}{j!(\alpha-j)!} = \frac{\Gamma(\alpha+1)}{\Gamma(k+1)\Gamma(\alpha-j+1)}, & j > 0 \\ 1, & j = 0 \end{cases} \tag{4}$$

$(-1)^j \binom{\alpha}{j}$ can be simplified using recursive methods as follows:

$$\omega_0^{(\alpha)} = 1,\ \omega_j^{(\alpha)} = \left(1 - \frac{\alpha+1}{j}\right) \omega_{j-1}^{(\alpha)}, j = 1,\ 2,\ 3 \cdots \tag{5}$$

The Grünwald–Letnikov derivative provides a difference-based approach to defining fractional-order derivatives, and this definition provides a powerful tool for describing and analyzing systems with complex dynamic behavior [35,36]. Therefore, the GL definition of the fractional-order model for predicting battery SOC is most applicable.

The continuous differential-integral can be defined as:

$${}_aD_t^\alpha = \begin{cases} \frac{d^\alpha}{dt^\alpha}, & \alpha > 0 \\ 1, & \alpha = 0 \\ \int_a^t (d\tau)^\alpha, & \alpha < 0 \end{cases} \tag{6}$$

In particular, the computational cost increases significantly when the step size h is small. In this study, while estimating the battery SOC using the UKF, the fractional-order model is updated with full parameters using the EKF, dramatically reducing the computational cost.

2.2. Fractional-Order Model

The fractional-order model offers a more precise representation of the complex electrochemical behavior and nonlinear characteristics of batteries, especially during the charge and discharge processes. In these processes, the relationship between internal current and

voltage often follows fractional-order dynamics, which traditional integer-order models struggle to fully capture. Common equivalent circuit models for batteries include the first-order Thevenin model and the second-order RC model. While the first-order RC model demands less computational power, it is generally suitable for systems exhibiting simple time constant behaviors, typically in linear and low-frequency applications. Lithium-ion batteries, however, present more complex dynamic behaviors during charging and discharging, including delays and phase shifts, which cannot be effectively captured by the first-order RC model. The second-order RC model, due to its superior stability, is widely employed in integer-order modeling of battery behavior [37]. The use of two RC networks provides a more precise representation of battery dynamics across different time scales. In the fractional-order model, the introduction of two capacitors, C1 and C2, along fractional-order operators α and β, forms a fractional-order network with two constant-phase elements (CPEs), as illustrated in Figure 1.

The fractional-order capacitive impedance can be expressed as:

$$\begin{cases} Z_{CPE1} = \frac{1}{(s^{\alpha}C1)} \\ Z_{CPE2} = \frac{1}{(s^{\beta}C2)} \end{cases} \tag{7}$$

The total impedance of the fractional-order model is:

$$Z_f = R_0 + \frac{1}{\frac{1}{R_1} + \frac{1}{Z_{CPE1}}} + \frac{1}{\frac{1}{R_2} + \frac{1}{Z_{CPE2}}} \tag{8}$$

where s is the complex frequency variable of the Laplace transform. α and β denote the orders of capacitors C1 and C2, respectively.

In addition, the resistance and the two sets of RC elements here are referred to as "ZARC", which are used to describe the frequency response characteristics of the battery in the mid-frequency region, particularly the charge transfer and double layer effects at the electrolyte interfaces. This model effectively captures the influence of nonlinear effects.

Using this model to capture the true behavior of batteries is challenged by systematic and measurement errors, given that the charge–discharge process involves intricate physicochemical reactions and is influenced by external factors such as time-dependent variables, uncertainties, and modeling inaccuracies. Additionally, the noise in the system is inherently unpredictable and non-Gaussian. Therefore, incorporating a novel tracking algorithm enables the system to manage complex, non-Gaussian noise under nonlinear operating conditions, as outlined in Section 3.

The battery SOC method is calculated using the ampere–time integration method:

$$SOC_k = SOC_{k-1} + \frac{\int_{k-1}^{k} \eta_k i(t) dt}{Q_N} \tag{9}$$

where $\boldsymbol{\eta_k}$ is the Coulombic efficiency and $\boldsymbol{Q_N}$ is the rated capacity of the battery. The battery capacity is obtained by charging the battery with constant current and constant voltage followed by the hybrid pulse power characterization (HPPC) discharge experiment, and the experimental steps are shown in Table 1. The average value of $\boldsymbol{Q_N}$ was obtained from three experiments as 6.5 Ah, and $\boldsymbol{\eta_k}$ = 0.95 was taken in this study.

Table 1. Intermittent discharge experimental procedure.

Step	Detailed Procedure
1	Charge the battery at constant current of 2 A and constant voltage of 4.2 V, respectively.
2	Discharge for 3 min with constant current of 6.5 A.
3	Leave the cell stationary for three hours to reach electrochemical equilibrium.
4	Repeat steps 2 and 3 until the cut-off voltage.

With the fractional-order model shown in Figure 1, the state space equations are established as follows:

$$\begin{bmatrix} \frac{d^{\alpha}}{dt^{\alpha}}\boldsymbol{U_1} \\ \frac{d^{\beta}}{dt^{\beta}}\boldsymbol{U_2} \end{bmatrix} = \begin{bmatrix} -\frac{1}{R_1C_1} & \mathbf{0} \\ \mathbf{0} & -\frac{1}{R_2C_2} \end{bmatrix} \begin{bmatrix} \boldsymbol{U_1} \\ \boldsymbol{U_2} \end{bmatrix} + \begin{bmatrix} \frac{1}{C_1} \\ \frac{1}{C_2} \end{bmatrix} \boldsymbol{I}(\boldsymbol{t}) \tag{10}$$

where $\boldsymbol{U_1}$ and $\boldsymbol{U_2}$ are the voltages across the RC network, respectively, and I(t) is the total battery current.

$\boldsymbol{U}(\boldsymbol{t})$ can be found in Kirchhoff's voltage law (KVL):

$$\boldsymbol{U}(\boldsymbol{t}) = [-\mathbf{1} - \mathbf{1}] \begin{bmatrix} \boldsymbol{U_1} \\ \boldsymbol{U_2} \end{bmatrix} - \boldsymbol{I}(\boldsymbol{t})\boldsymbol{R_0} + \boldsymbol{U_{OCV}} \tag{11}$$

$\boldsymbol{U_{OCV}}$ indicates the end cell voltage (OCV) associated with the SOC.

The discrete fractional-order nonlinear model of the state space equation is as follows:

$$\begin{aligned} \boldsymbol{x_k} &= \boldsymbol{A_{k-1}x_{k-1}} + \boldsymbol{B_{k-1}I_{k-1}} + \boldsymbol{\omega_{k-1}} - \sum_{j=1}^{k} \boldsymbol{K_j x_{k-1}} \\ \boldsymbol{U_k} &= \boldsymbol{C_k x_k} - \boldsymbol{I_k R_0} + \boldsymbol{E} + \boldsymbol{\nu_k} \end{aligned} \tag{12}$$

where $\boldsymbol{A_{k-1}} = \boldsymbol{diag}\left\{-\frac{h^{\alpha}}{R_1C_1}, -\frac{h^{\beta}}{R_2C_2}, \mathbf{1}\right\}$, $\boldsymbol{B_{k-1}} = \boldsymbol{diag}\left[\frac{h^{\alpha}}{C_1}, \frac{h^{\beta}}{C_2}, -\frac{\eta_{k-1}h}{Q_N}\right]^T$, $\boldsymbol{C_{k-1}} = [-\mathbf{1}, -\mathbf{1}, \mathbf{0}]$, and the state vector $\boldsymbol{x_k} = \left[\boldsymbol{U_1}(\boldsymbol{k}), \boldsymbol{U_2}(\boldsymbol{k}), \boldsymbol{SOC}(\boldsymbol{k})\right]^{\boldsymbol{T}}$. $\boldsymbol{\omega_k}$ and $\boldsymbol{\nu_k}$ are the system process noise and observation noise, respectively.

2.3. Fractional-Order Model Parameter Identification

Accurate parameter identification is essential for effective battery state of charge (SOC) prediction using the fractional-order model. This study employs the whale optimization algorithm (WOA) for offline parameter identification, with the results serving as initial values for the fractional-order model. These initial values are subsequently updated through online parameter identification using the extended Kalman filter (EKF). Specifically, the WOA is used to identify parameters for the fractional-order model, including $\boldsymbol{R_1}$, $\boldsymbol{R_2}$, $\boldsymbol{C_1}$, $\boldsymbol{C_2}$, $\boldsymbol{\alpha}$ and $\boldsymbol{\beta}$.

In the WOA, adjusting the control coefficients for the contraction-enclosure and exploration phases allows the algorithm to alternate between contraction-enclosure and random search modes. This flexibility enables the algorithm to adapt effectively across different search stages.

When $|a| < 1$, the algorithm mainly performs shrink-wrap operations:

$$\mathbf{X}(\boldsymbol{t}+\mathbf{1}) = \mathbf{X}(\boldsymbol{t}) - \boldsymbol{a}\cdot|\boldsymbol{c}\cdot\mathbf{X}(\boldsymbol{t}) - \mathbf{X}(\boldsymbol{t})| \tag{13}$$

When $|a| \geq 1$, the algorithm then randomly chooses to perform a global search:

$$\mathbf{X}(\boldsymbol{t}+\mathbf{1}) = \mathbf{X}_{\boldsymbol{rand}} - \boldsymbol{a}\cdot|\boldsymbol{c}\cdot\mathbf{X}_{\boldsymbol{rand}} - \mathbf{X}(\boldsymbol{t})| \tag{14}$$

The difference between the predicted voltage and the actual voltage is used to measure the fitness function, which can be defined as:

$$\boldsymbol{J}(\boldsymbol{i}) = \sum_{\boldsymbol{i}=\mathbf{1}}^{\boldsymbol{T}+\mathbf{1}} \left(\boldsymbol{U_{ekf}}(\boldsymbol{i}) - \boldsymbol{U_{ot}}(\boldsymbol{i})\right)^{\mathbf{2}} \tag{15}$$

where $\boldsymbol{U_{ekf}}(\boldsymbol{i})$ is the voltage at the ith time point through the fractional-order model and $\boldsymbol{U_{ot}}(\boldsymbol{i})$ is the voltage at the ith time point actually measured. T represents the number of sampling time points.

The degree of adaptation can be expressed as:

$$fit = \frac{J_{max} - J(i)}{\sum_{i=1}^{N}(J_{max} - J(i))} \tag{16}$$

where J_{max} denotes the maximum value of the fitness function.

2.4. Analysis of Fractional-Order Model Parameter Identification Results

Simulations were conducted using MATLAB R2023b software, setting the population size to 300, with a termination condition of an error of less than 0.008 V, using a data set of 120,000 data points. The results of parameter identification are shown in Table 2.

Table 2. Fractional-order model parameter identification results.

Model	R_0	R_1	R_2	C_1	C_2	α	β
FOM	0.0286 Ω	0.0100 Ω	0.0398 mΩ	2.7626 kF	280.54 kF	0.9039	0.9819

In the fractional-order second-order RC model, the parameters are designed to simulate the dynamic characteristics of the battery's charge and discharge processes based on its electrochemical behavior. Specifically, R_1 represents the polarization resistance of the battery, which is associated with the battery's energy storage and release characteristics. This resistance is typically larger in magnitude. R_2, on the other hand, generally represents the ohmic resistance (internal resistance) of the battery, which reflects the direct opposition to current flow and is usually smaller in value.

The capacitors C_1 and C_2 in the model represent the battery's energy storage capability. The core of the fractional-order model lies in the fractional-order operators α and β, which influence the system's response speed and dynamic characteristics. By incorporating these fractional-order parameters, the model is able to more accurately capture the nonlinear and hysteretic effects present in the battery during its charge and discharge cycles.

2.5. Model Accuracy Validation

The accuracy of the WOA is validated by comparing the terminal voltages predicted by the identified fractional-order models with the actual measured voltages. Additionally, the results are compared with those obtained using the integer-order second-order RC model. The comparisons are presented in Figures 2 and 3.

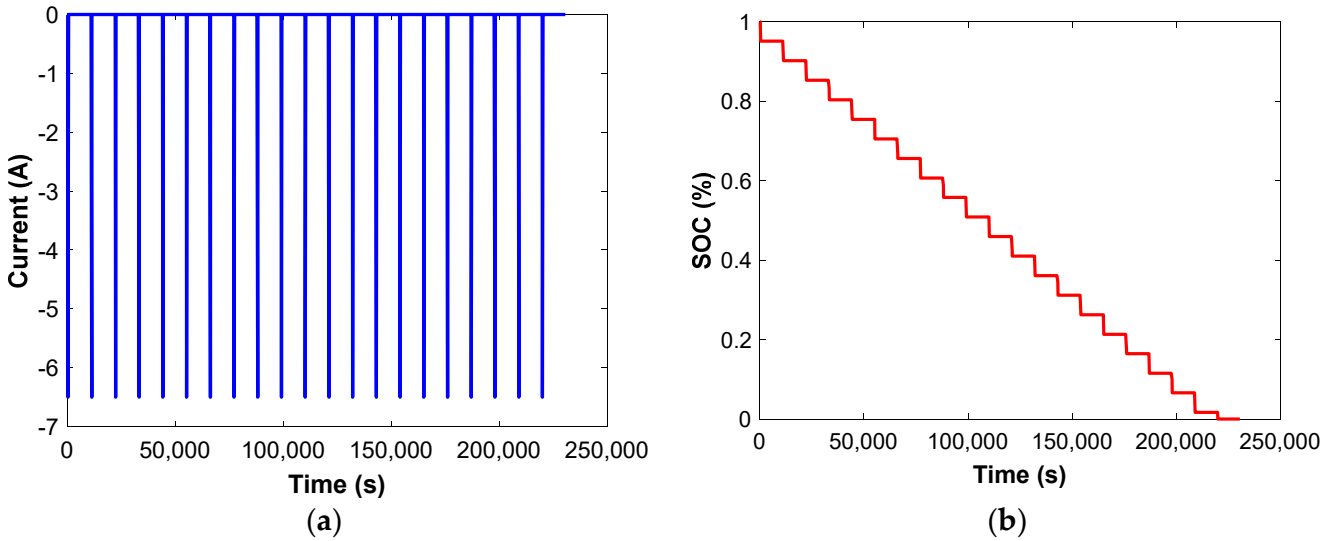

Figure 2. HPPC impulse test current test. (**a**) Current curve; (**b**) SOC curve.

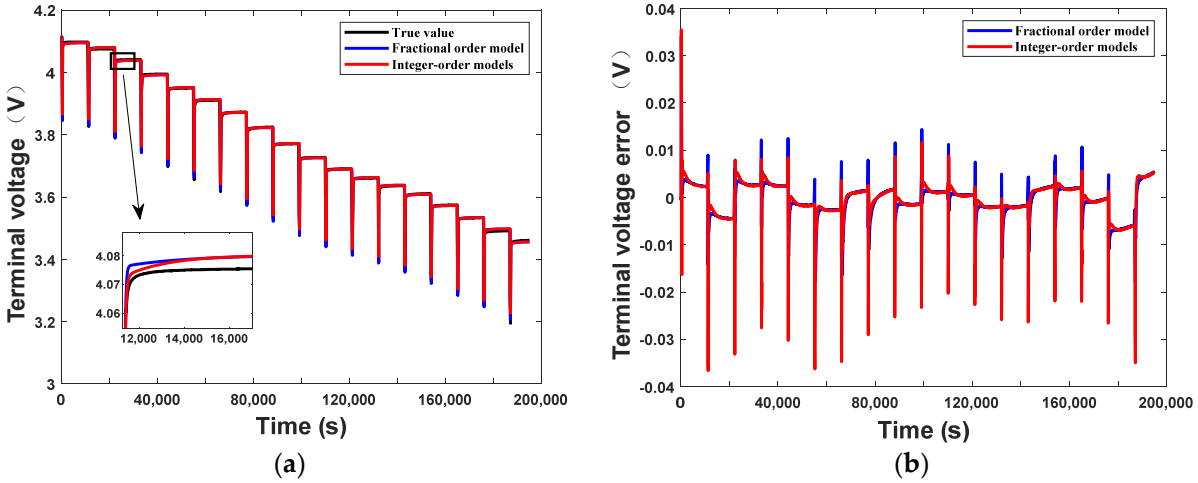

Figure 3. Model identification results. (**a**) End voltage comparison; (**b**) end voltage error comparison.

The fractional-order model, by incorporating fractional-order integral terms, can provide a smoother estimation of the battery's state of charge (SOC), avoiding the significant fluctuations or errors typically observed in integer-order models during the later stages of discharge. This mitigates the issue of inaccurate SOC estimation caused by end-voltage errors. As illustrated in the figure, the fractional-order model better captures the electrochemical processes of the battery, with errors noticeably smaller than those of the integer-order model. The maximum voltage difference between the two models reached 0.03 V. Specific evaluation metrics are shown in Table 3.

Table 3. Model evaluation indicators.

Model	Average Error	Maximum Error
IOM	0.0027 V	0.0366 V
FOM	0.0025 V	0.0340 V

3. Fractional-Order-Model-Based Strong Tracking Multi-Neo-Interest Adaptive Untraceable Kalman Method (FOMIST-AUKF-EKF)

3.1. Fractional-Order Traceless Kalman Filter Algorithm

The nonlinear system (12) can be expressed as:

$$\begin{cases} x_{k+1} = F(x_k, u_{k+1}) + \omega_k \\ y_k = G(x_k, u_k) + v_k \end{cases} \tag{17}$$

Setting the initial state and state error covariance:

$$\hat{x}_{0,0}^{+} = E\left[U_{1,2}, \hat{z}_0^{+}\right], P_{x_{0,0}}^{+} = E\left[\left(x_{0,0} - \hat{x}_{0,0}^{+}\right)\left(x_{0,0} - \hat{x}_{0,0}^{+}\right)^T\right] \tag{18}$$

where $\hat{x}_{0,0}^{+}$ and $P_{x_{0,0}}^{+}$ are the initial putative values and the error covariance matrix.

Step 1: For k = 1, 2, 3. . .. . ., calculation:

(1) Update prior estimation.

(2) Create sigma points at time step k − 1:

$$\begin{cases} \hat{\boldsymbol{x}}_{k-1,l}^{0} = \hat{\boldsymbol{x}}_{k-1}^{+} + \overset{\wedge}{\boldsymbol{x}}_{l}^{(i)} \\ \hat{\boldsymbol{x}}_{k-1}^{+} = \overset{\wedge}{\boldsymbol{x}}_{k-1}^{(i)} + \left(\sqrt{(j+\lambda)P_{k-1}^{+}}\right)_i, i = 1,\ 2, \ldots,\ j \\ \overset{\wedge}{\boldsymbol{x}}_{k-1}^{(i)} = \overset{\wedge}{\boldsymbol{x}}_{k-1}^{(i)} - \left(\sqrt{(j+\lambda)P_{k-1}^{+}}\right)_i, i = j+1, j+2, \ldots, 2j \end{cases} \tag{19}$$

where k is the time step, λ is the scaling factor, α is a scale factor, and j is the quantity of state variables. Particularly, $\lambda = \alpha^2(j+k) - j,\ \alpha = 0.01$.

(3) Calculate the weights:

$$\begin{cases} w_m^{(0)} = \lambda/(j+\lambda) \\ w_c^{(0)} = \lambda/(n+\lambda) + \left(1-\alpha^2+\beta\right) \\ w_m^{(\mathrm{i})} = w_c^{(\mathrm{i})} = 1/(2(n+\lambda)) \end{cases} \tag{20}$$

where β is the coefficient corresponding to the type of noise.

(4) Update prior state value $\hat{x}_{k,l}^{-}$:

$$\hat{x}_{k,l}^{-} = f\left(\hat{x}_{k,l-1}^{i}, \hat{x}_{k}^{-}, u_{k,l}\right) = \sum_{i=0}^{2n} \omega_m^i \hat{\mathrm{x}}_{k,l}^{i} - \sum_{j=1}^{k} K_j \hat{\mathrm{x}}_{k,l-j}^{+} \tag{21}$$

(5) Update state error covariance $P_{x_{k,l}}^{-}$:

$$P_{x_{k,l}}^{-} = \sum_{i=0}^{2n} \omega_c^i \left(\hat{\mathrm{x}}_{k,l}^{i} - \hat{\mathrm{x}}_{k,l}^{-}\right)\left(\hat{\mathrm{x}}_{k,l}^{i} - \hat{\mathrm{x}}_{k,l}^{-}\right)^T + Q_{k,l} \tag{22}$$

Step 2: Observation estimation:

Convert sigma points into observation estimation points:

$$\hat{y}_{k,l}^{i} = g(\hat{x}_{k,l}^{i}, \hat{\theta}_{k}^{-}, u_{k,l}) \tag{23}$$

where $g(.)$ represents the observation models.

And then:

$$\hat{\mathrm{y}}_{k,l}^{-} = \sum_{i=0}^{2n} \omega_m^i \hat{\mathrm{y}}_{k,l}^{i} \tag{24}$$

Calculating covariance matrix:

$$P_y^{-} = \sum_{i=0}^{2n} \omega_c^i \left(\hat{\mathrm{y}}_{k,l}^{i} - \hat{\mathrm{y}}_{k,l}^{-}\right)\left(\hat{\mathrm{y}}_{k,l}^{i} - \hat{\mathrm{y}}_{k,l}^{-}\right)^T + R_{k,l} \tag{25}$$

$$P_{xy}^{-} = \sum_{i=0}^{2n} \omega_c^i \left(\hat{x}_{k,l}^{i} - \hat{x}_{k,l}^{-}\right)\left(\hat{y}_{k,l}^{i} - \hat{\mathrm{y}}_{k,l}^{-}\right)^T \tag{26}$$

Calculating the Kalman gain:

$$K_k = \frac{P_{xy}}{P_y} \tag{27}$$

Posterior estimation update:

Updating the states and covariance:

$$\hat{x}_{k,l}^{+} = \hat{x}_{k,l}^{-} + K_k\left(y_{k,l} - \hat{y}_{k,l}^{-}\right) \tag{28}$$

$$P_{xk,l}^{+} = P_{xk,l}^{-} - K_k P_y K_k^T \tag{29}$$

3.2. Improved SOC Prediction Method Based on Fractional-Order Model

3.2.1. Multi-Innovation-Based FOUKF (FOMI-UKF)

In practical operating conditions, observed measurements are often affected by noise and environmental disturbances, and relying on a single observation can lead to significant

deviations due to these influences. By incorporating multiple innovations, a combination of information from various observations can be utilized to reduce state estimation errors and enhance filtering accuracy.

The multi-innovation algorithm introduces multiple innovations in both the observation update and state update processes of the FOUKF algorithm, as illustrated below:

Multi-New Interest Observation Update:

Consider that there are m observations $z_{k,1}, z_{k,2}, \ldots, z_{k,m}$. Define the new rate $\nu_{k,j}$ as the error of the j th observation:

$$\nu_{k,j} = z_{k,j} - g(\hat{x}{}^{i}_{k,l}, \overset{\wedge}{\theta}{}^{-}_{k}, u_{k,l}) \tag{30}$$

Equation (25) Kalman gain K_k update is modified to $K_{j,k}$:

$$K_{j,k} = \left[K_{1,k}, K_{2,k}, \cdots K_{p,k}\right] \tag{31}$$

The covariance matrix is updated to:

$$P^{+}_{xk,l} = P^{-}_{xk,l} - \Sigma^{m}_{j=1} K_{j,k} P_y K^{T}_{j,k} \tag{32}$$

Weighted update of state estimates using multiple new interest:

$$\hat{x}_{k|k} = \hat{x}_{k|k-1} + \Sigma^{m}_{j=1} \lambda_j K_{k,j} \nu_{k,j} \tag{33}$$

Adding weighting factors to the state estimates at different moments can adjust the balance between historical information and current observations. For FOMI-UKF, the state weighting factors are as follows:

$$\begin{cases} \lambda_1 = 0.2 \\ \lambda_2 = \lambda_3 = \cdots \lambda_m = \frac{1-\lambda_1}{m-1}, 0 \le a \le 1 \end{cases} \tag{34}$$

where m is the length of the innovation. Although multi-neo-interest coupling can increase the estimation accuracy, adding more information will undoubtedly increase the computational cost, so this study sets the value of m to 18.

3.2.2. Fractional-Order Strong-Tracking Multi-Neo-Interest Traceless Kalman Filter Algorithm (FOMIST-UKF)

UKF modeling of observation and process noise relies heavily on the accuracy of the covariance matrix. However, extreme operating currents or high noise levels can lead to unstable UKF estimates and low convergence rates, resulting in significant estimation errors and lags.

The strong tracking filter adjusts the filter gain during the state estimation process to respond quickly to sudden and nonlinear changes in the system state, thus enhancing the convergence ability of the filter.

FOMISTFUKF dynamically adjusts the covariance matrix by introducing a tracking factor λ_k. One of the substantial tracking factors is as follows:

$$\lambda_k = \begin{cases} \lambda_{0,k} & \lambda > 1 \\ 1 & \lambda \le 1 \end{cases} \tag{35}$$

Among them:

$$\lambda_{0,k} = \frac{Tr(P^{x}_{y})}{Tr(P^{+}_{xk,l})} \tag{36}$$

where $Tr(P_y^x)$ is the trace of the P_y^x matrix, and the statistical width of P_y^x is obtained from the true value of the number m of new interest. When the trace factor $\lambda > 1$, a real-variable asymptotic cancelation factor $\lambda_{0,k}$ is introduced; when the strong trace factor $\lambda \leq 1$, the prediction is made according to the normal UKF.

3.2.3. Fractional-Order Multi-Innovation Strongly Tracking Adaptive Traceless Kalman Filter Algorithm (FOMIST-AUKF)

The conventional UKF relies on a pre-set process noise variance matrix Q_k and observation noise matrix R_k. If the initial values are set too high or too low, the predicted results will be dispersed, and the noise characteristics under realistic operating conditions will change over time.

The adaptive UKF uses the statistical properties of the new interest vector to estimate the adjustment R_k and the adjustment Q_k using the process residuals as follows:

Calculate the sample covariance of the information P_ν:

$$\mathbf{P}_\nu = \frac{1}{k}\sum_{i=1}^{k} \nu_{i,j}{\nu_{i,j}}^T \tag{37}$$

Update the observation noise covariance matrix R_k:

$$\mathbf{R}_k = \beta \mathbf{R}_{k-1} + (1-\beta)\mathbf{P}_y \tag{38}$$

where β is a forgetting factor for smoothing updates and $0 < \beta < 1$.

Calculate the process residuals e_k and the sample covariance P_e:

$$\mathbf{e}_k = \hat{x}_{k|k} - \hat{x}_{k|k-1} \tag{39}$$

$$\mathbf{P}_e = \frac{1}{k}\sum_{i=1}^{k} \mathbf{e}_i \mathbf{e}_i^T \tag{40}$$

Update process noise covariance matrix Q_k.

$$\mathbf{Q}_k = \gamma \mathbf{Q}_{k-1} + (1-\gamma)\mathbf{P}_e \tag{41}$$

where γ is a forgetting factor for smoothing updates and $0 < \gamma < 1$.

The new interest vector ν_k and the process residual e_k reflect the errors in the observations as well as in state prediction, and the adaptive tuning of R and Q allows the filter to adapt more accurately to changes in the noise characteristics of the system and reduce the resulting estimation errors.

3.3. Fractional-Order Strong-Tracking Multi-Neo-Interest Adaptive Traceless Kalman Filter Algorithm with EKF Joint Estimation (FOMIST-AUKF-EKF)

Realistic battery operating conditions usually have nonlinear characteristics, and the parameters of the battery will change with factors such as discharge multiplication and battery aging, so fixed battery parameters cannot accurately reflect the current state of the battery. Therefore, updating the estimated battery parameters online in real time is necessary.

This study extends the FOMIST-AUKF using the EKF to provide more accurate parameter estimates for the system. The specific methodology is as follows:

Initialization: parameter estimation vector $\hat{\theta}_0$, covariance matrix $\mathbf{P}_\theta(0)$, process noise and measurement noise covariance matrices $\mathbf{Q}_\theta$ and $\mathbf{R}_\theta$.

Parameter status update:

$$\mathbf{z}_k = \begin{bmatrix} \mathbf{x}_k \\ \theta_k \end{bmatrix} \tag{42}$$

State prediction for extended states:

$$\hat{\mathbf{z}}_{k|k-1} = \begin{bmatrix} \hat{\mathbf{x}}_{k|k-1} \\ \hat{\theta}_{k|k-1} \end{bmatrix} \tag{43}$$

Updated based on observations:

$$\hat{\mathbf{y}}_{k,\theta} = h(\hat{\mathbf{x}}_{k|k-1}, \hat{\theta}_{k|k-1}) \tag{44}$$

System linearization:

$$\mathbf{F}_{\theta} = \frac{\partial f(\hat{x}_{k|k}, \mathrm{R}_{k-1}, \theta)}{\partial \theta}|_{\hat{\theta}_{k-1}} \tag{45}$$

The Kalman gain is calculated as follows:

$$\mathbf{K}_k = \mathbf{P}_{\theta,k-1}\mathbf{H}^{\top}(\mathbf{H}\mathbf{P}_{\theta,k|k-1}\mathbf{H}^{\top} + \mathbf{R})^{-1} \tag{46}$$

where $\mathbf{H}^{\top}$ is the transpose of the observation matrix.

Prediction parameter covariance:

$$\mathbf{P}_{\theta,k} = \mathbf{P}_{\theta,k-1} + \mathbf{Q}_{\theta} \tag{47}$$

Prediction parameter status:

$$\hat{\mathbf{z}}_{k|k} = \hat{\mathbf{z}}_{k|k-1} + \mathbf{K}_k(\mathbf{y}_k - \hat{\mathbf{y}}_k) \tag{48}$$

The detailed steps of the FOMIST-AUKF-EKF algorithm are as follows (see Figure 4):

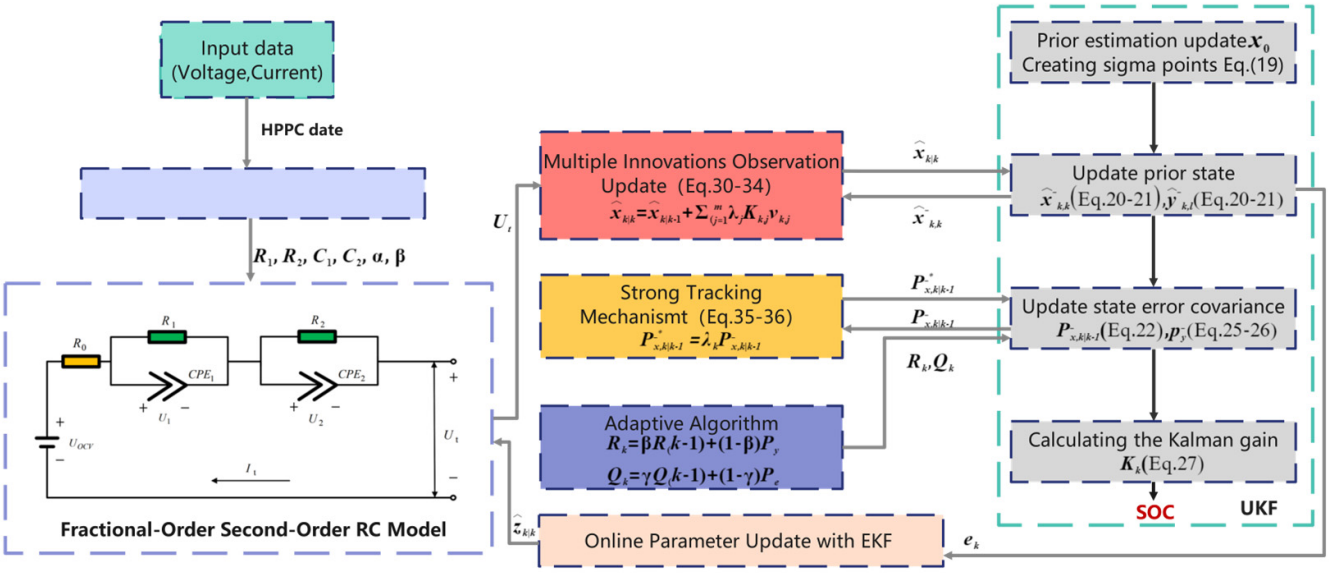

Figure 4. FOMIST-AUKF-EKF process.

4. Experimental Simulation Verification of Working Conditions

4.1. Experimental Platforms

The experimental platform of this study was carried out on battery test apparatus (Neware CT-4008Tn-5V12A-S1). The precision error of this testing instrument is 0.05%, the thermostat (Neware MGDW-225-20) is controlled at 25 °C, and the working condition platform is shown in Figure 5. The test was conducted under the New European Driving Cycle (NEDC) condition (Figure 6a) and the driving situation tracking test (DST) condition (Figure 6b).

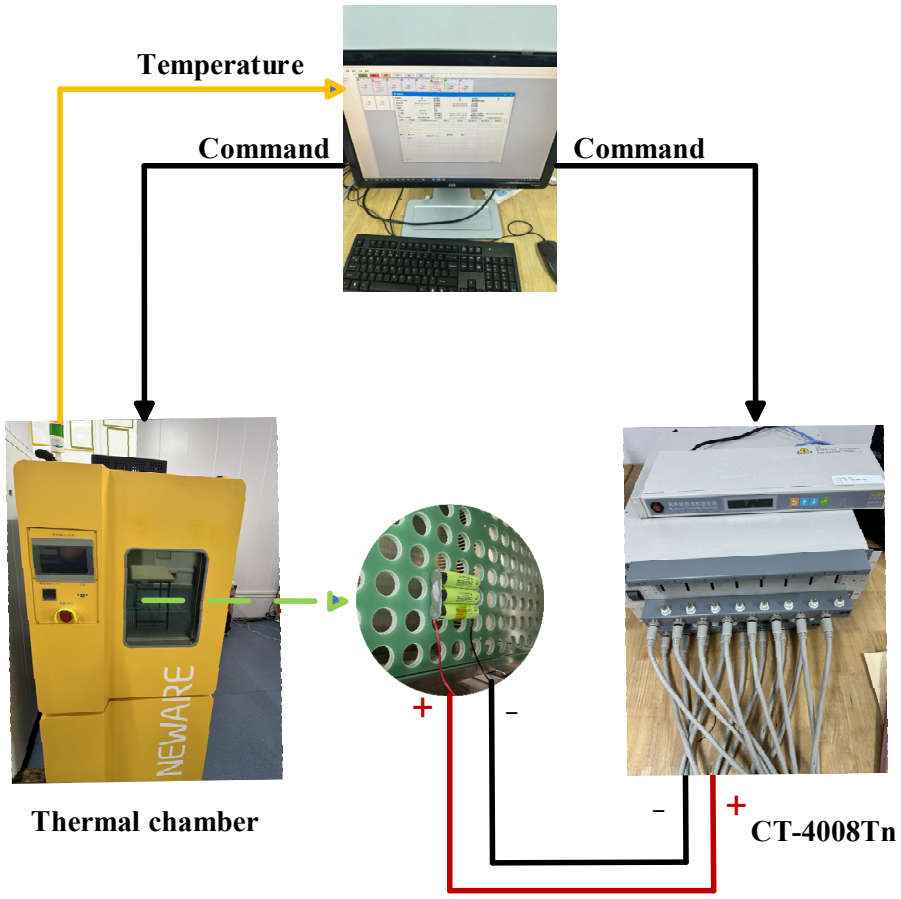

Figure 5. Battery experiment platform.

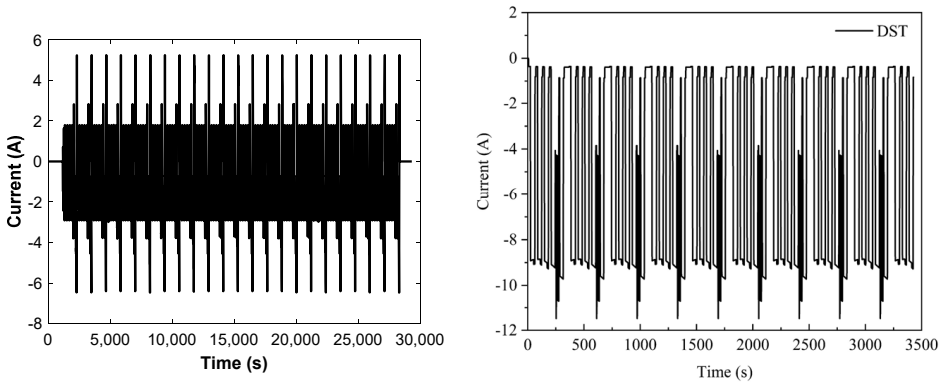

Figure 6. (**a**) Current map of NEDC working condition; (**b**) current map of DST working end.

4.2. Condition Test

In order to verify the robustness and stability of FOMISTFAUKF-EKF, the experiments were conducted to compare UKF, FOUKF, FOMI-UKF, FOMIST-UKF, FOMIST-AUKF, and FOMIST-AUKF+EKF, respectively.

The test state indicators MAE and RMSE are calculated as follows:

$$MAE = \frac{1}{n}\sum_{i=1}^{n} | x_i - \hat{x}_i | \tag{49}$$

$$RMSE = \sqrt{\frac{1}{n}\sum_{k=1}^{n}(U_t - U_e)^2} \tag{50}$$

As shown in Figure 6a,b, the FOMISTFAUKF-EKF algorithm's SOC estimation results and SOC error are presented under the NEDC conditions. Figure 7c,d illustrate the predicted end voltage and its associated error. Under the NEDC scenario, the FOMIST-AUKF-EKF algorithm achieves a mean absolute error (MAE) of 0.018% and a root mean square error (RMSE) of 0.56% in SOC prediction. The algorithm maintains high accuracy even under extreme current conditions, primarily due to the strong tracking mechanism (Equation (33)), which enables rapid adjustment to observation errors, effectively reducing SOC estimation errors caused by load variations. The introduction of multi-sensor fusion further enhances the accuracy of the estimates by updating the voltage values as per Equation (31), thereby mitigating estimation bias caused by individual measurement errors. The MAE of the end voltage is 0.0061 V, with a maximum error of only 0.1054 V. The results are shown in Table 4.

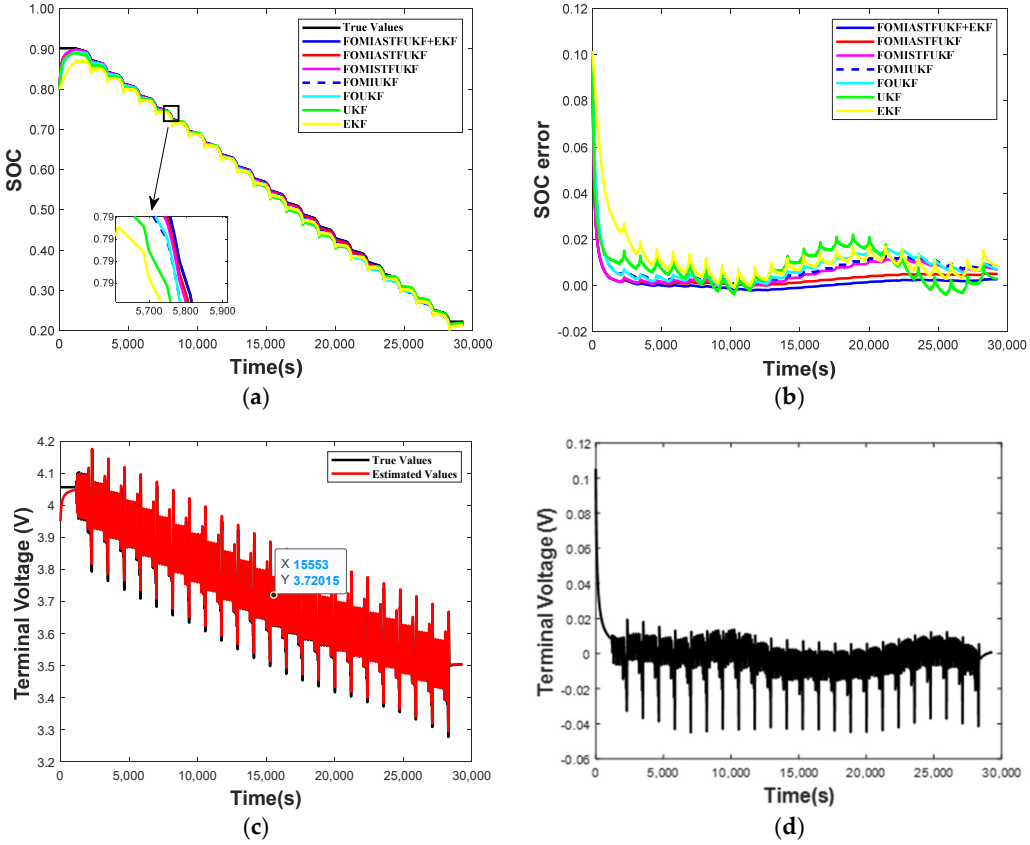

Figure 7. NEDC operating conditions. (**a**) SOC comparison; (**b**) SOC error comparison; (**c**) end voltage comparison; (**d**) end voltage error.

Table 4. Errors of each algorithm under NEDC conditions.

Method	NEDC						
	FOMIASTFAUKF+EKF	**FOMIASTFUKF**	**FOMISTFUKF**	**FOMIUKF**	**FOUKF**	**UKF**	**EKF**
Average Error (%)	0.13	0.25	0.50	0.63	0.69	0.74	0.87
Maximum Error (%)	0.27	0.51	1.17	1.31	1.65	2.20	2.71

The FOMIST-AUKF-EKF algorithm predicts a MAE of 0.28% and RMSE of 1.21% for SOC under DST condition. The detailed results are presented in Figure 8 and Table 5: the terminal voltage MAE is 0.0117 V with a maximum error of only 0.1825 V. This shows that the investigated method is also robust as well as convergent to extreme currents for complex conditions. In particular, the MAEs of FOUKF and UKF are 1.65% and 2.20%,

respectively, which fully demonstrate that the fractional-order model is more accurate than the integer-order model in describing the battery interior under the fractional-linear operating conditions.

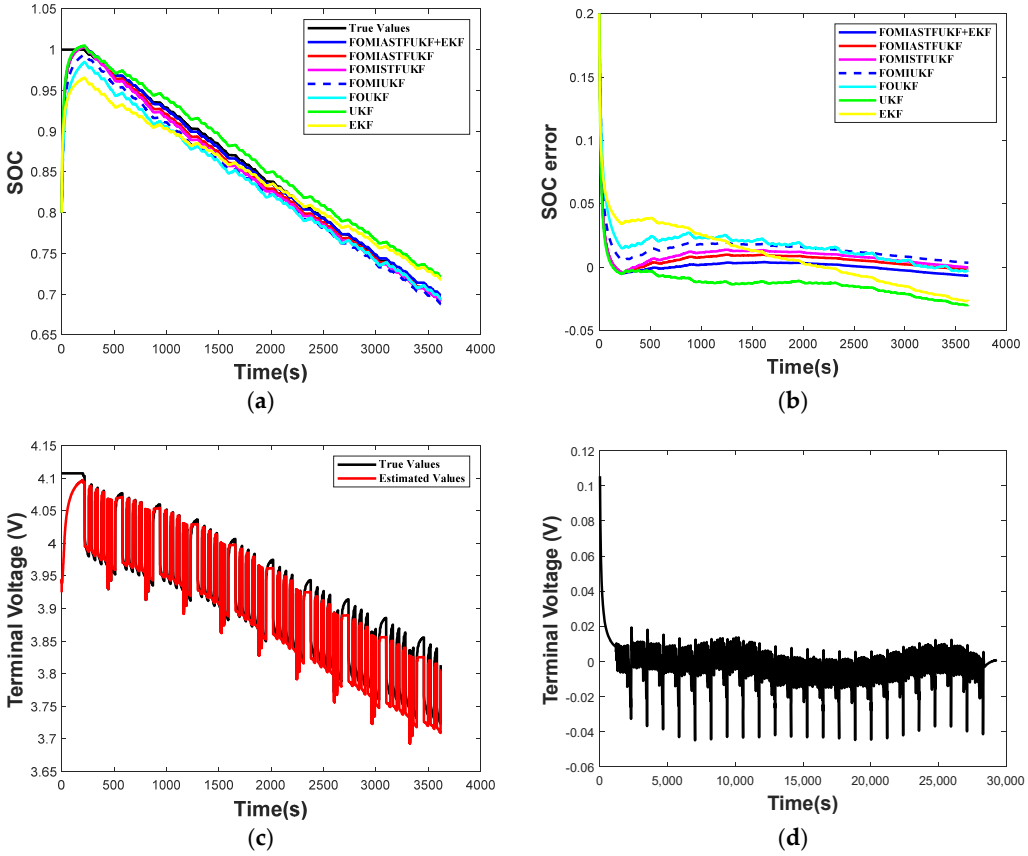

Figure 8. (**a**) SOC comparison; (**b**) SOC error comparison; (**c**) terminal voltage comparison; (**d**) terminal voltage error under DST operating conditions.

Table 5. Errors of each algorithm under DST conditions.

Method	DST						
	FOMIASTFAUKF+EKF	**FOMIASTFUKF**	**FOMISTFUKF**	**FOMIUKF**	**FOUKF**	**UKF**	**EKF**
Average Error (%)	0.27	0.58	0.87	1.34	1.43	1.53	1.60
Maximum Error (%)	0.67	1.00	1.39	1.96	2.74	2.98	3.90

Accurate SOC estimation is indispensable for real-time parameter updating, and in this study, EKF is used to jointly estimate the battery parameters, which reduces the computational burden and strikes a balance between accuracy and computational complexity. The real-time update estimation of battery model parameters by FOMISTFAUKF-EKF under NEDC conditions is shown in Figures 9–11. In particular, the ohmic resistance of a battery, R_0, typically reflects the voltage drop of the battery during a fast response, and R_0 has a direct effect on the transient change in current.

As the battery is used, the activity of the electrode material gradually decreases, resulting in an increase in the ohmic resistance R_0. R_1 and R_2 correspond to the polarization resistance of the battery at different time constants, respectively, and they increase with the thickening of the SEI film of the battery. The capacitance C_1, C_2 is related to the polarization effect of the cell, and the capacitance parameters generally do not change significantly with cell aging, especially in the early and middle part of the cell life, so the C_1, C_2 values as well as the fractional order α, β do not change significantly.

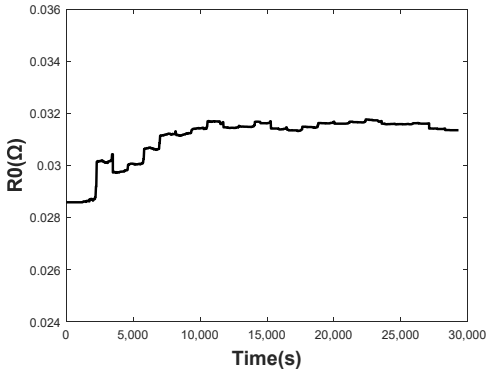

Figure 9. Change in ohmic resistance R_0.

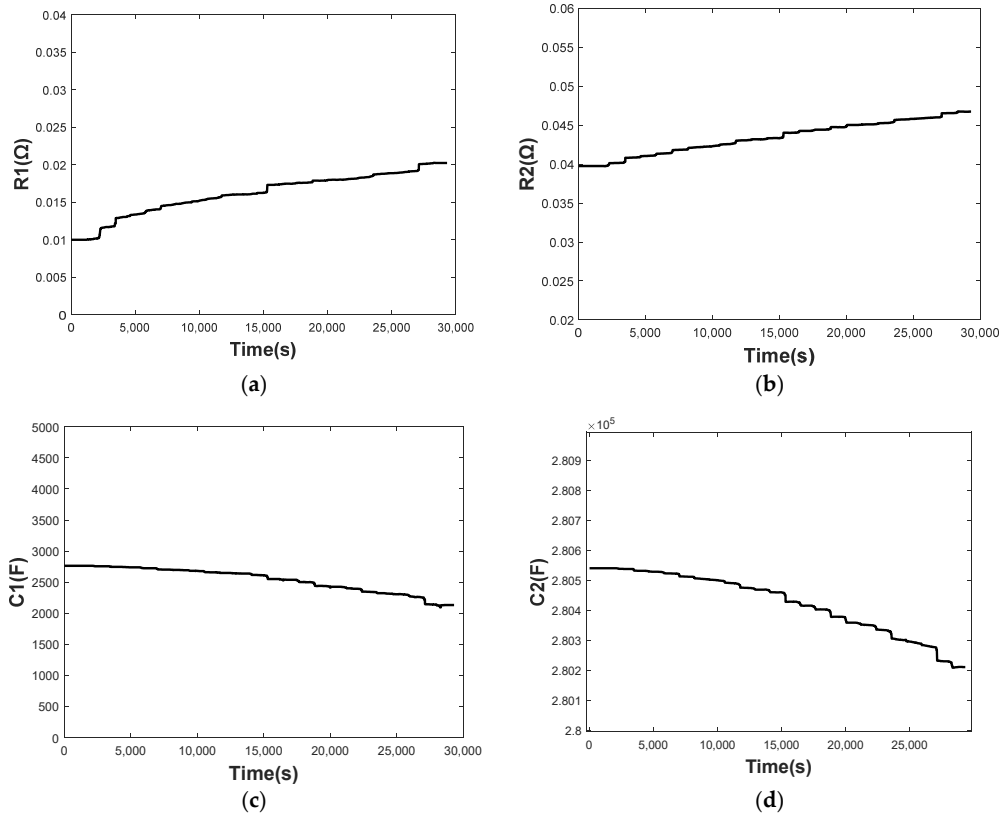

Figure 10. Parameter identification and update results of second-order RC network. (**a**) Change in ohmic resistance R_1 (**b**) Change in ohmic resistance R_2 (**c**) Change in ohmic resistance C_1 (**d**) Change in ohmic resistance C_2.

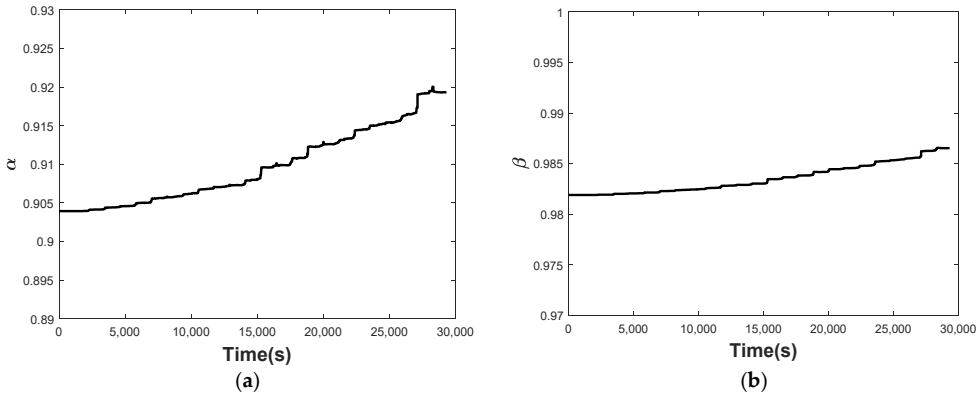

Figure 11. (**a**) Fractional-order parameters α and (**b**) identification results β.

5. Conclusions

This paper proposes an improved UKF-EKF joint estimation algorithm based on fractional-order models. By incorporating multiple hibernation filters, this approach overcomes the limitations of updating the system with single-time measurements, thereby enhancing SOC estimation accuracy. A strong tracking filtering algorithm is integrated, allowing the Kalman filter to quickly respond to abrupt changes through an adaptive gain adjustment mechanism. Additionally, an adaptive algorithm is employed, enabling the filter to continuously adjust the noise covariance matrix based on real-time measurement data. This dynamic adaptation to the system's noise characteristics ensures robust filtering performance. The EKF achieves precise SOC estimation through full-parameter joint estimation for the fractional-order model. The algorithm was validated under two operating conditions, NEDC and DST, with MAE values of 0.018% and 0.28%, respectively, demonstrating the accuracy and feasibility of the proposed method.

For future work, additional sensor data, such as temperature, will be incorporated into the model. This will involve the development of a temperature-dependent model that accounts for real-time temperature variations. By introducing a temperature compensation mechanism, based on the dynamic characteristics of the battery's thermal behavior, the aim is to further enhance the accuracy and reliability of SOC estimation.

Author Contributions: Conceptualization, Y.L. and J.W.; methodology, L.Z.; software, Y.Z.; validation, J.W., Q.S. and Y.Z.; formal analysis, J.W.; data curation, Q.S.; writing—original draft preparation, Y.L.; writing—review and editing, J.X.; visualization, Q.S.; supervision, L.Z. All authors have read and agreed to the published version of the manuscript.

Funding: This work was supported by the Hainan Province Key R&D Program Projects (ZDYF2023GXJS148), Haikou Key Science and Technology Programs (220-034), and Hainan Provincial Natural Science Foundation High-level Talent Program (521RC497), for supporting this research.

Data Availability Statement: Data will be made available on request.

Conflicts of Interest: The authors declare no conflicts of interest.

Nomenclature

BMS	Battery management system	NEDC	New European Driving Cycle
SOC	State of charge	DST	Dynamic stress test
SOH	State of health	OCV	Open-circuit voltage
KF	Kalman filter	2RC	Second-order RC
UKF	Unscented Kalman filter	RMSE	Root mean square error
HKF	Hybrid Kalman filter	MAE	Mean absolute error
EKF	Extended Kalman filter	ME	Mean error
AUKF	Adaptive unscented Kalman filter	FO-MIST	Fractional-order multiple innovation strong tracking
		HPPC	Hybrid pulse power characterization

References

1. Amrouche, S.O.; Rekioua, D.; Rekioua, T.; Bacha, S. Overview of energy storage in renewable energy systems. *Int. J. Hydrogen Energy* **2016**, *41*, 20914–20927. [CrossRef]
2. Diouf, B.; Pode, R. Potential of lithium-ion batteries in renewable energy. *Renew. Energy* **2015**, *76*, 375–380. [CrossRef]
3. Gabbar, H.A.; Othman, A.M.; Abdussami, M.R. Review of battery management systems (BMS) development and industrial standards. *Technologies* **2021**, *9*, 28. [CrossRef]
4. Chen, L.; Wu, X.; Machado, J.A.T.; Lopes, A.M.; Li, P.; Dong, X. State-of-charge estimation of lithium-ion batteries based on fractional-order square-root unscented Kalman filter. *Fractal Fract.* **2022**, *6*, 52. [CrossRef]
5. Wu, L.; Lyu, Z.; Huang, Z.; Zhang, C.; Wei, C. Physics-based battery SOC estimation methods: Recent advances and future perspectives. *J. Energy Chem.* **2023**, *89*, 27–40. [CrossRef]
6. Zou, C.; Klintberg, A.; Wei, Z.; Fridholm, B.; Wik, T.; Egardt, B. Power capability prediction for lithium-ion batteries using economic nonlinear model predictive control. *J. Power Sources* **2018**, *396*, 580–589. [CrossRef]
7. Allagui, A.; Freeborn, T.J.; Elwakil, A.S.; Fouda, M.E.; Maundy, B.J.; Radwan, A.G.; Said, Z.; Abdelkareem, M.A. Review of fractional-order electrical characterization of supercapacitors. *J. Power Sources* **2018**, *400*, 457–467. [CrossRef]

8. Sabatier, J.; Cugnet, M.; Laruelle, S.; Grugeon, S.; Sahut, B.; Oustaloup, A.; Tarascon, J. A fractional order model for lead-acid battery crankability estimation. *Commun. Nonlinear Sci. Numer. Simul.* **2010**, *15*, 1308–1317. [CrossRef]
9. Hussein, H.M.; Esoofally, M.; Donekal, A.; Rafin, S.M.S.H.; Mohammed, O. Comparative Study-Based Data-Driven Models for Lithium-Ion Battery State-of-Charge Estimation. *Batteries* **2024**, *10*, 89. [CrossRef]
10. Koehler, J.; Soloperto, R.; Muller, M.A.; Allgower, F. A computationally efficient robust model predictive control framework for uncertain nonlinear systems. *IEEE Trans. Autom. Control* **2020**, *66*, 794–801. [CrossRef]
11. Nguyen, T.H.; Bui, D.Q.; Dao, P.N. An efficient Min/Max Robust Model Predictive Control for nonlinear discrete-time systems with dynamic disturbance. *Chaos Solitons Fractals* **2024**, *180*, 114551. [CrossRef]
12. Chai, X.; Li, S.; Liang, F. A novel battery SOC estimation method based on random search optimized LSTM neural network. *Energy* **2024**, *306*, 132583. [CrossRef]
13. Mastali, M.; Vazquez-Arenas, J.; Fraser, R.; Fowler, M.; Afshar, S.; Stevens, M. Battery state of the charge estimation using Kalman filtering. *J. Power Sources* **2013**, *239*, 294–307. [CrossRef]
14. Sepasi, S.; Ghorbani, R.; Liaw, B.Y. Improved extended Kalman filter for state of charge estimation of battery pack. *J. Power Sources* **2014**, *255*, 368–376. [CrossRef]
15. He, H.; Xiong, R.; Peng, J. Real-time estimation of battery state-of-charge with unscented Kalman filter and RTOS μCOS-II platform. *Appl. Energy* **2016**, *162*, 1410–1418. [CrossRef]
16. Lee, J.; Nam, O.; Cho, B.H. Li-ion battery SOC estimation method based on the reduced order extended Kalman filtering. *J. Power Sources* **2007**, *174*, 9–15. [CrossRef]
17. Chen, C.; Xiong, R.; Yang, R.; Shen, W.; Sun, F. State-of-charge estimation of lithium-ion battery using an improved neural network model and extended Kalman filter. *J. Clean. Prod.* **2019**, *234*, 1153–1164. [CrossRef]
18. Mu, H.; Xiong, R.; Zheng, H.; Chang, Y.; Chen, Z. A novel fractional order model based state-of-charge estimation method for lithium-ion battery. *Appl. Energy* **2017**, *207*, 384–393. [CrossRef]
19. Jin, G.; Li, L.; Xu, Y.; Hu, M.; Fu, C.; Qin, D. Comparison of SOC estimation between the integer-order model and fractional-order model under different operating conditions. *Energies* **2020**, *13*, 1785. [CrossRef]
20. Lai, X.; He, L.; Wang, S.; Zhou, L.; Zhang, Y.; Sun, T.; Zheng, Y. Co-estimation of state of charge and state of power for lithium-ion batteries based on fractional variable-order model. *J. Clean. Prod.* **2020**, *255*, 120203. [CrossRef]
21. Sethia, G.; Nayak, S.K.; Majhi, S. An approach to estimate lithium-ion battery state of charge based on adaptive Lyapunov super twisting observer. *IEEE Trans. Circuits Syst. I Regul. Pap.* **2020**, *68*, 1319–1329. [CrossRef]
22. Geng, X.; He, X.; Hu, M.; Bi, M.; Teng, X.; Wu, C. Multi-attention network with redundant information filtering for multi-horizon forecasting in multivariate time series. *Expert Syst. Appl.* **2024**, *257*, 125062. [CrossRef]
23. Ren, X.; Li, C.; Ma, X.; Chen, F.; Wang, H.; Sharma, A.; Gaba, G.; Masud, M. Design of multi-information fusion based intelligent electrical fire detection system for green buildings. *Sustainability* **2021**, *13*, 3405. [CrossRef]
24. Baros, J.; Sotola, V.; Bilik, P.; Martinek, R.; Jaros, R.; Danys, L.; Simonik, P. Review of fundamental active current extraction techniques for SAPF. *Sensors* **2022**, *22*, 7985. [CrossRef] [PubMed]
25. Wang, J.; Wen, T.; Cai, B.; Roberts, C. A high-order strong tracking filter based on a compensated adaptive model for predicting sudden changes in remaining useful life of a lithium-ion battery. *J. Energy Storage* **2024**, *88*, 111494. [CrossRef]
26. Ghosh, S.; Das, S.; Roy, S.; Islam, S.M.; Suganthan, P. A differential covariance matrix adaptation evolutionary algorithm for real parameter optimization. *Inf. Sci.* **2012**, *182*, 199–219. [CrossRef]
27. Fan, X.; Feng, H.; Yun, X.; Wang, C.; Zhang, X. SOC estimation for lithium-ion battery based on AGA-optimized AUKF. *J. Energy Storage* **2024**, *75*, 109689. [CrossRef]
28. Fu, Y.; Zhai, B.; Shi, Z.; Liang, J.; Peng, Z. State of charge estimation of lithium-ion batteries based on an adaptive iterative extended Kalman filter for AUVs. *Sensors* **2022**, *22*, 9277. [CrossRef]
29. Zeng, J.; Wang, S.; Zhang, M.; Cao, W.; Fernandez, C.; Guerrero, J.M. Battery multi-time scale fractional-order modeling method for state of charge estimation adaptive to full parameters updating. *J. Energy Storage* **2024**, *86*, 111283. [CrossRef]
30. Beelen, H.; Bergveld, H.J.; Donkers MC, F. Joint estimation of battery parameters and state of charge using an extended Kalman filter: A single-parameter tuning approach. *IEEE Trans. Control Syst. Technol.* **2020**, *29*, 1087–1101. [CrossRef]
31. Li, L.; Liu, J.G. A generalized definition of Caputo derivatives and its application to fractional ODEs. *SIAM J. Math. Anal.* **2018**, *50*, 2867–2900. [CrossRef]
32. Jiang, Y.; Zhang, B. Comparative study of Riemann–Liouville and Caputo derivative definitions in time-domain analysis of fractional-order capacitor. *IEEE Trans. Circuits Syst. II Express Briefs* **2019**, *67*, 2184–2188. [CrossRef]
33. Chatterjee, S.; Biswas, S.; Majee, A.; Sen, S.; Oliva, D.; Sarkar, R. Breast cancer detection from thermal images using a Grunwald-Letnikov-aided Dragonfly algorithm-based deep feature selection method. *Comput. Biol. Med.* **2022**, *141*, 105027. [CrossRef] [PubMed]
34. Verma, P.; Kumar, M. Analytical solution with existence and uniqueness conditions of non-linear initial value multi-order fractional differential equations using Caputo derivative. *Eng. Comput.* **2022**, *38*, 661–678. [CrossRef]
35. Sarfraz, M.; Zhou, J.; Ali, F. An 8D Hyperchaotic System of Fractional-Order Systems Using the Memory Effect of Grünwald–Letnikov Derivatives. *Fractal Fract.* **2024**, *8*, 530. [CrossRef]
36. Zafar, Z.U.A.; Ali, N.; Zaman, G.; Thounthong, P.; Tunç, C. Analysis and numerical simulations of fractional order Vallis system. *Alex. Eng. J.* **2020**, *59*, 2591–2605. [CrossRef]

37. Hannan, M.A.; Lipu, M.S.H.; Hussain, A.; Mohamed, A. A review of lithium-ion battery state of charge estimation and management system in electric vehicle applications: Challenges and recommendations. *Renewable and Sustainable Energy Rev.* **2017**, *78*, 834–854. [CrossRef]